The Astrophysical Journal, 784:136 (11pp), 2014 April 1 doi:10.1088/0004-637X/784/2/136

COROTATING SOLAR WIND STRUCTURES AND RECURRENT TRAINS OF ENHANCED DIURNAL VARIATION IN GALACTIC COSMIC RAYS

T. Yeeram[1,2], D. Ruffolo[1,2], A. Sáiz[1,2], N. Kamyan[1,2], and T. Nutaro[2,3]
[1] Department of Physics, Faculty of Science, Mahidol University, Bangkok 10400, Thailand; thana.thana@hotmail.com, david.ruf@mahidol.ac.th, alejandro.sai@mahidol.ac.th, p_chang24@hotmail.com
[2] Thailand Center of Excellence in Physics, CHE, Ministry of Education, Bangkok 10400, Thailand
[3] Department of Physics, Faculty of Science, Ubon Ratchathani University, Ubon Ratchathani 34190, Thailand; tnutaro@yahoo.com
Received 2013 November 22; accepted 2014 February 23; published 2014 March 14

ABSTRACT

Data from the *Princess Sirindhorn Neutron Monitor* at Doi Inthanon, Thailand, with a vertical cutoff rigidity of 16.8 GV, were utilized to determine the diurnal anisotropy (DA) of Galactic cosmic rays (GCRs) near Earth during solar minimum conditions between 2007 November and 2010 November. We identified trains of enhanced DA over several days, which often recur after a solar rotation period (∼27 days). By investigating solar coronal holes as identified from synoptic maps and solar wind parameters, we found that the intensity and anisotropy of cosmic rays are associated with the high-speed streams (HSSs) in the solar wind, which are in turn related to the structure and evolution of coronal holes. An enhanced DA was observed after the onset of some, but not all, HSSs. During time periods of recurrent trains, the DA was often enhanced or suppressed according to the sign of the interplanetary magnetic field **B**, which suggests a contribution from a mechanism involving a southward gradient in the GCR density, n, and a gradient anisotropy along $\mathbf{B} \times \nabla n$. In one non-recurrent and one recurrent sequence, an HSS from an equatorial coronal hole was merged with that from a trailing mid-latitude extension of a polar coronal hole, and the slanted HSS structure in space with suppressed GCR density can account for the southward GCR gradient. We conclude that the gradient anisotropy is a source of temporary changes in the GCR DA under solar minimum conditions, and that the latitudinal GCR gradient can sometimes be explained by the coronal hole morphology.

Key words: cosmic rays – interplanetary medium – solar wind

1. INTRODUCTION

During solar minimum conditions, near the minimum of the solar activity cycle (sunspot cycle), there are large-scale three-dimensional corotating solar wind structures that persist quasi-periodically in the heliosphere and corotate with the Sun with a period of about 27 days. These include expanding high-speed streams (HSSs) with speeds of about 450–800 km s^{-1} from coronal holes (CHs), and the preceding corotating interaction regions (CIRs) where the HSSs interact with slow-speed streams. The CHs are large-scale regions of low-density plasma and open magnetic field lines, typically with a single polarity toward or away from the Sun. The pattern of the coronal magnetic field extends into interplanetary space as carried out by the solar wind. Consequently, the global pattern of CHs and their magnetic polarity is mapped into the spatial structure of the interplanetary field that rotates with the Sun (e.g., Hundhausen et al. 1980) with a pattern of alternating sectors where the magnetic field is toward or away from the Sun as observed at Earth orbit. Large polar CHs predominate during much of the solar cycle, and may migrate to low latitudes extending across the solar equator (Zirker 1977). Furthermore, an HSS may be observed near the solar equatorial plane even for a high-latitude CH. When a CIR passes the Earth, an observer can see also a sharp increase in solar wind speed followed by a slow decrease until a new CIR arrives. The CIR appears to be corotating with the Sun since the CH-HSS structure is usually stable for more than one solar rotation. Since these HSSs and CIRs are quasi-periodic, large-scale structures in interplanetary space, they have significant effects on temporal and spatial variations of Galactic cosmic rays (GCRs) that enter the inner heliosphere.

Roughly speaking, a faster solar wind speed can inhibit the entry of GCRs to the inner heliosphere, and is typically associated with a reduced GCR flux. Thus corotational variations in solar wind speed are associated with well-known "synodic" or "27 day variations" in the GCR flux (Fonger 1953; Simpson 1998; da Silva et al. 2007), which have sometimes been called "recurrent Forbush decreases." An HSS causes a temporary cosmic ray decrease, either due to shielding by the CIR (Heber et al. 1999; Richardson 2004) or due to a change in particle diffusion properties in local interplanetary space in low and middle heliolatitudes (Chih & Lee 1986; Kóta & Jokipii 1991). The temporary reduction of the GCR flux is followed by a recovery phase in the trailing portion of the HSS.

Diurnal variations of GCRs (Hess & Graziadei 1936) have also been observed to be affected by HSSs and CIRs according to the 27 day period of solar rotation with "recurrent tendencies" (Pomerantz & Duggal 1971). Variations in the GCR flux have commonly been observed by ground-based detectors, such as neutron monitors and muon detectors, that measure count rates of secondary particles from cosmic ray interactions (showers) in Earth's atmosphere. Diurnal variations arise from the Earth's rotation as a ground-based detector's viewing direction sweeps through the sky with a one day period. Cosmic rays of energy up to ∼100 GeV are affected by the Sun and the interplanetary magnetic field (IMF), which introduces an energy-dependent anisotropy (Rao 1972). Then the anisotropic flow of cosmic rays is clearly manifest as a diurnal variation of the count rates at ground level. The average diurnal anisotropy (DA) vector has been explained as a consequence of the equilibrium established between the radial convection of the cosmic ray particles by solar wind and the inward diffusion of GCR particles along the IMF (see Rao 1972; Forman & Gleeson 1975). In a reference frame corotating with the Sun, convection and parallel diffusion (i.e., diffusion parallel to the large-scale magnetic field) can nearly cancel and the GCR distribution has almost no net flow. Then in

Earth's reference frame, there is a net flow as the corotating GCR distribution impinges on Earth from the dusk sector. Without drifts or perpendicular diffusion, the streaming is observed as an average corotational anisotropy along the direction of the Earth's orbit. Transient variations are superimposed on the steady state corotational anisotropy, and they sometimes form "trains" of enhanced diurnal variation that persist for several consecutive days (Duldig & Humble 1990 and references therein).

The causes of the trains of enhanced diurnal variations in GCR intensity in association with HSSs and CIRs are not yet completely understood. Mori et al. (1975) reported a strong dependence of these recurrences on the sector structure of the IMF during 1973–1975. The average amplitudes of DA and semi-DA were found to be larger than normal during the initial phase of the stream but smaller than normal during the decreasing phase of the stream, and the phase (time of peak flux, which corresponds to a direction in space) was observed to remain almost constant at around 1800 LT (Iucci et al. 1983). Munakata et al. (2003) used 17 neutron monitors and 17 components of the Nagoya muon telescope, with median rigidities between ∼10 GV and ∼120 GV. They reported diurnal amplitudes observed by neutron monitors that were enhanced during the period of decline of the HSS, which might be associated with the recovery of the cosmic ray intensity. For 1991–1994, Mishra & Mishra (2005) have studied the high-amplitude anisotropic wave train events and found that the phase of the diurnal variations for a majority of events shifted toward later hours, whereas it remained at the corotational hour for some events. Mavromichalaki (1989) investigated neutron monitor data of 1970–1977 and found that the phase shifted toward earlier hours, perhaps in association with variation of the size of the polar CHs, an effect in agreement with the drift motions of cosmic ray particles in the IMF. By investigating the differences in the areas of the solar polar CHs and their relationship with the cosmic ray intensity as measured by neutron monitors (Thule and McMurdo), the hemisphere having a CH of larger area exhibited a lower cosmic ray intensity than the opposite hemisphere (Agrawal et al. 1978, 1980). The authors attributed this to convective removal of cosmic rays produced by the higher-speed solar wind streams associated with the larger CH. Singh et al. (2010) reported that HSSs did not play any significant role in causing high- and low-amplitude wave train events and the phase did not shift to earlier hours, but the DA decreased during the solar activity minima in 2008. Variations in GCR intensity and anisotropy have also been analyzed in terms of a 27 day periodicity, which provides a statistical description of the effects of HSSs and CIRs. For example, Owens et al. (1980) provided evidence for a gradient anisotropy along $\mathbf{B} \times \nabla n$ due to gradients in the GCR density n. Gil et al. (2012) examined the dependence on solar magnetic polarity and found the DA variation to be consistent with a drift model of solar modulation, while the intensity variation did not follow a consistent pattern. In summary, effects of the HSSs and CIRs on the trains of enhanced diurnal variations are still an open issue and causes of these effects need to be clarified.

The present work aims to characterize trains of enhanced and suppressed DA of GCRs, and their recurrence with a roughly 27 day period. Section 2 presents observations and analysis of cosmic ray data from the *Princess Sirindhorn Neutron Monitor* (*PSNM*) at Doi Inthanon, Thailand, along with interplanetary plasma data and synoptic maps of the solar corona during the recent solar minimum. Section 3 presents an analysis of trains and recurrent trains of enhanced and suppressed DA in which the DA often exhibited magnetic-sector dependence. We propose a gradient anisotropy to explain this effect and select case studies of trains to study in more detail. We present examples in which unusually strong diurnal variations can be explained in terms of the gradient anisotropy along $\mathbf{B} \times \nabla n$, e.g., as associated with a particular type of CH morphology. These results are discussed in Section 4.

2. OBSERVATIONS AND DATA ANALYSIS

2.1. Cosmic Rays

Cosmic ray data in this study were obtained from the *PSNM*, which houses an 18-tube neutron monitor of the standard NM64 design. The *PSNM* is located at the summit of Doi Inthanon, Thailand's highest mountain, at an altitude of about 2560 m and geographic coordinates 18.°59N and 98.°49E. The vertical cutoff rigidity of 16.8 GV is the highest for any fixed neutron monitor station in the world. For a GCR proton at the vertical cutoff rigidity the Larmor radius would be 0.08 AU in a 5 nT magnetic field. The hourly pressure corrected data from Doi Inthanon for 2007 November to 2010 November, representing solar minimum conditions, have been subjected to harmonic analysis, removing a 24 hr running average. The days with more than 3 hr of missing data were discarded from the study and gaps up to 3 hr were filled in by interpolation. From this method, we have determined the resultant amplitude and time of maximum of the GCR DA.

In our harmonic analysis, for each day (in universal time, UT) the fractional excess count rate F as a function of time was analyzed for its harmonic component at a frequency $\omega = 2\pi/(8.64 \times 10^4$ s), i.e., 2π radians day^{-1}:

$$F_\omega(t) = D_x \cos \omega t + D_y \sin \omega t, \quad (1)$$

where D_x and D_y are the components of the DA and t is the time since the start of the day in UT.

During the time period of our analysis, the effects of large cosmic ray intensity perturbations such as Forbush decreases due to coronal mass ejections were not present.

2.2. Interplanetary Plasma

We utilized the 1 hr averaged interplanetary plasma data from the MAG and SWEPAM instruments of the *Advanced Composition Explorer* (*ACE*)[4] and the OMNI Web site.[5] We define the polarity sector of the IMF based on hourly mean IMF components in Geocentric Solar Ecliptic (GSE) coordinates, for which the x-axis points from the Earth to the Sun, the z-axis points along ecliptic north, and the y-axis completes the right-handed system. The sectors of IMF toward (the Sun) and away (from the Sun) are defined relative to a plane normal to the nominal 45° Parker spiral mean field direction in the ecliptic plane; i.e., the IMF is designated toward (T) if $B_x > B_y$ and away (A) if $B_y > B_x$.

Solar wind structure is characterized by the solar wind plasma parameters. HSSs are identified as regions of solar wind speed $V_{SW} \geqslant 450$ km s^{-1}. Each stream has a specific polarity, and magnetic sector boundaries are often found close to compression regions. CIRs have well-known characteristics such as an increase in density and magnetic field magnitude at the leading edge of a HSS, or an increase in thermal speed after the stream interface inside a CIR (Burlaga 1974).

[4] http://www.srl.caltech.edu/ACE/ASC/level2/index.html
[5] http://omniweb.gsfc.nasa.gov/

2.3. Synoptic Maps

The evolution and features of the CHs are characterized by utilizing Fe XII 195 Å synoptic maps[6] for 40 Carrington rotations (CRs; from CR2064 to CR2103) from the Extreme Ultraviolet Imager (EUVI) of the Sun Earth Connection Coronal and Heliospheric Investigation (SECCHI; Howard et al. 2008) on the *Solar TErrestrial RElations Observatory* (*STEREO*) spacecraft (Kaiser et al. 2008). We have examined data from both *STEREO* spacecraft, *STEREO-A* (Ahead) and *STEREO-B* (Behind), but in this report we show only data from *STEREO-A*.

In order to compare the synoptic maps with the cosmic ray flux and plasma parameters measured at or near Earth we have to correct for the observing angle of (in this case) *STEREO-A*. First, we assumed that the solar wind speed is constant from the source to the Earth (ballistic mapping back in time). The position data in GSE coordinates of *STEREO-A*[7] were employed to calculate the longitudinal separation between Earth and *STEREO-A*, which monotonically increased during the period of our study, from 20° in 2007 November to 82° in 2010 November. In this study, for the sake of simplicity we neglected the small longitudinal separation between the *ACE* spacecraft and Earth. When comparing data from *PSNM* and *ACE* with a synoptic chart from *STEREO-A*, we must shift the latter to account for the solar wind travel time to Earth and the longitudinal separation, $\Delta\varphi$,

$$\Delta t = \frac{1\ \mathrm{AU}}{V_{ACE}} - \frac{\Delta\varphi}{\Omega_\odot}, \quad (2)$$

where V_{ACE} is the solar wind speed as observed by *ACE*, and for the average synodic rotation frequency of solar magnetic features we use $\Omega_\odot = 2\pi/26.75$ radians day^{-1} (Bai 1987).

In addition, we considered latitudinal excursions of the heliospheric current sheet (HCS) as derived from Potential Field Source Surface (PFSS) analysis of Wilcox Solar Observatory (WSO) magnetograms.[8] In PFSS analysis the coronal magnetic field is calculated from photospheric field observations with a potential field model. The field is forced to be radial at the source surface (2.5 R_S) to approximate the effect of the accelerating solar wind on the field configuration (Schatten et al. 1969).

3. RESULTS AND DISCUSSION

3.1. Statistics of the Diurnal Variation at Doi Inthanon

The harmonic analysis using data from the *PSNM* at Doi Inthanon from 2007 November to 2010 November resulted in mean values $\langle D_x \rangle = -0.0002$ (s.d. = 0.0009) and $\langle D_y \rangle = 0.0013$ (s.d. = 0.0011). Interpreting (D_x, D_y) as a harmonic vector, the mean value has a magnitude $D = 0.0013$ (s.d. = 0.0011) and phase 1.7 radians (s.d. = 0.7). In other words, the mean diurnal variation was 0.13%. This phase implies a maximum diurnal enhancement at 6.6 hr UT. Doi Inthanon is located at longitude 98°.49E, so the true local time (LT) is UT + 6.57 hr, and the diurnal enhancement peaks at 13.1 hr LT. Based on particle tracing through Earth's magnetic field (Lin et al. 1995) and using the response function of Nagashima et al. (1989), coupling coefficients are determined. The coupling coefficient for the amplitude, 0.67, indicates that the asymptotic direction of peak DA is close to the Equator, and there is a phase shift of 62°.5 from the longitude of Doi Inthanon (T. Kuwabara 2010, private communication). This phase shift implies a peak flux from the direction of 17.3 hr LT, close to the corotational direction, 18 hr LT (Rao 1972). Based on the coupling coefficients, the mean value of D implies a mean anisotropy of 0.20% in the near-Earth cosmic ray flux above the cutoff rigidity. All the DA values reported in Table 1 and the figures are already corrected for the coupling coefficient and phase shift.

Table 1
Trains of Enhanced Diurnal Variation at Doi Inthanon from 2007 November to 2010 November[a]

Year	Days of Year	Duration	Diurnal Variation		Time of Maximum
	(DOY)	(days)	Max (%)	Mean (%)	Mean ± s.d. (hr LT)
2007	309–318	10	0.63	0.40	15.8 ± 1.8
2007	351–359	9	0.52	0.34	18.5 ± 2.1
2008	*94–103*	*10*	*0.40*	*0.32*	*17.6 ± 1.8*
2008	*125–135*	*11*	*0.53*	*0.37*	*18.0 ± 2.2*
2008	*176–196*	*21*	*0.79*	*0.45*	*17.8 ± 1.4*
2008	*203–209*	*7*	*0.46*	*0.37*	*17.1 ± 1.4*
2008	*219–225*	*7*	*0.61*	*0.40*	*16.1 ± 2.5*
2009	107–115	9	0.42	0.32	17.5 ± 0.8
2010	*1–11*	*11*	*0.38*	*0.30*	*15.2 ± 1.3*
2010	*34–42*	*9*	*0.53*	*0.39*	*16.8 ± 1.6*
2010	*48–56*	*9*	*0.75*	*0.55*	*15.9 ± 1.0*
2010	*75–88*	*14*	*0.54*	*0.42*	*17.9 ± 1.0*
2010	*112–119*	*8*	*0.63*	*0.55*	*16.3 ± 1.3*
2010	*139–148*	*10*	*0.64*	*0.46*	*16.8 ± 1.9*
2010	*154–172*	*19*	*0.74*	*0.49*	*17.3 ± 1.1*
2010	*186–201*	*16*	*0.50*	*0.40*	*16.9 ± 2.1*
2010	250–259	10	0.70	0.60	18.1 ± 2.1

Note. [a] Italicized data refer to recurrent trains.

3.2. Trains and Recurrent Trains of Enhanced and Suppressed Diurnal Variations

Trains of enhanced DA from 2007 November to 2010 November are listed in Table 1, some of which are recurrent. The trains of enhanced DA were chosen according to a criterion of DA $\geqslant$ 0.25% for a duration $\geqslant$7 days (about one-quarter of a 27 day rotation). We observed two periods of recurrent trains of suppressed and enhanced DAs that roughly repeat after a 27 day CR, from CR2068 to CR2073 (Figure 1) and from CR2092 to CR2098 (Figure 2). The trains of enhanced DA usually start within a few days from the start of an HSS and a depressed GCR flux. Furthermore, the recurrent DAs seem to be magnetic-sector dependent, where the enhanced DAs were mostly in the A sectors and the suppressed ones were mostly in the T sectors.

During the first period of recurrent trains, in CR2068–CR2073 during 2008 (Figure 1), the intensity of GCRs usually decreased near the start of an HSS around day 5 of the CR, which was often near the leading edge of a T sector. Note that such recurrent GCR decreases during HSSs represent the well known 27 day variations (Fonger 1953; Simpson 1998). The intensity then recovered completely or partially, mostly before the trailing edge of the stream. This recurrent HSS in the T sector exhibited recurrent trains of enhanced DA only during CR2072–CR2073. Another HSS came on day 12 or 13 of every CR, during the A sector, causing another temporary decrease in GCRs and usually exhibiting a recurrent train of enhanced DA. These trains of enhanced DA were always in the A sector, except during days of year (DOY) 186–196 and 219–224, when the HCS was close to the heliolatitude of Earth, as we shall discuss in Section 3.4.1.

[6] http://secchi.nrl.navy.mil/synomaps/index.php?p=cmnumber.php
[7] http://www.srl.caltech.edu/STEREO/attorb.html
[8] http://wso.stanford.edu/synsourcel.html

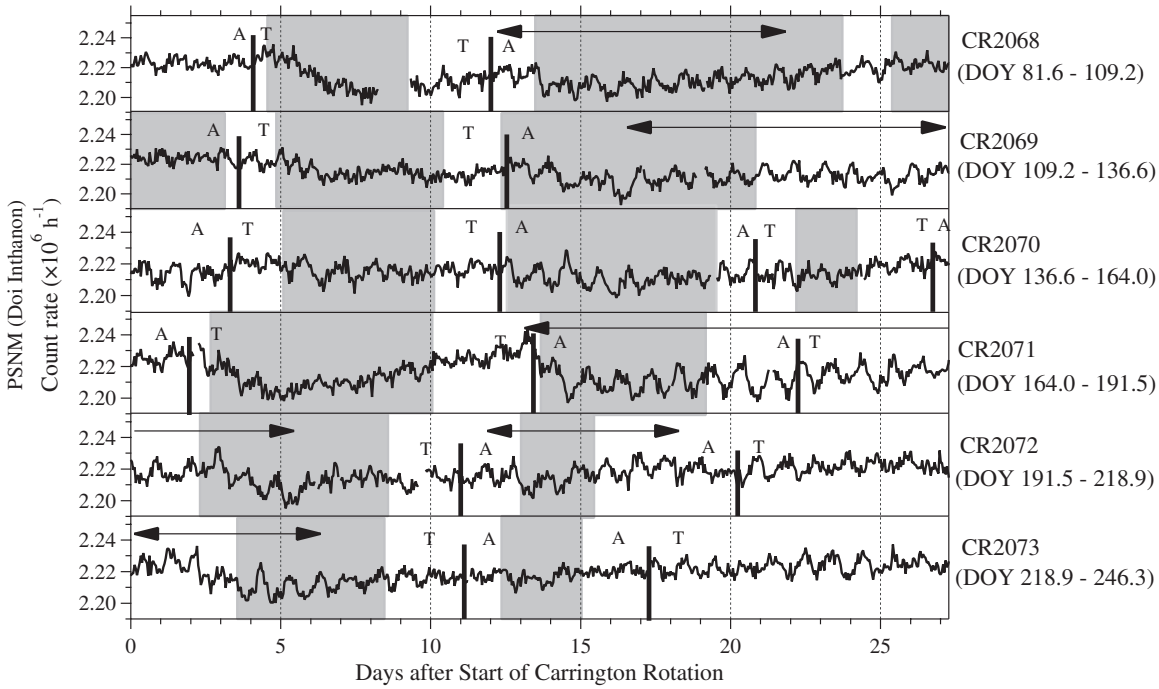

Figure 1. Count rate of the *Princess Sirindhorn Neutron Monitor* at Doi Inthanon as a function of time, showing recurrent trains of enhanced diurnal anisotropy (DA) in 2008, indicated by arrows, compared with magnetic sectors (toward, T, or away, A) for six successive CRs, CR2068–CR2073. Shaded areas represent HSSs with solar wind speed $\geqslant$450 km s^{-1}. Recurrently enhanced DA was often observed in the A sector, while suppressed DA was often observed in the T sector.

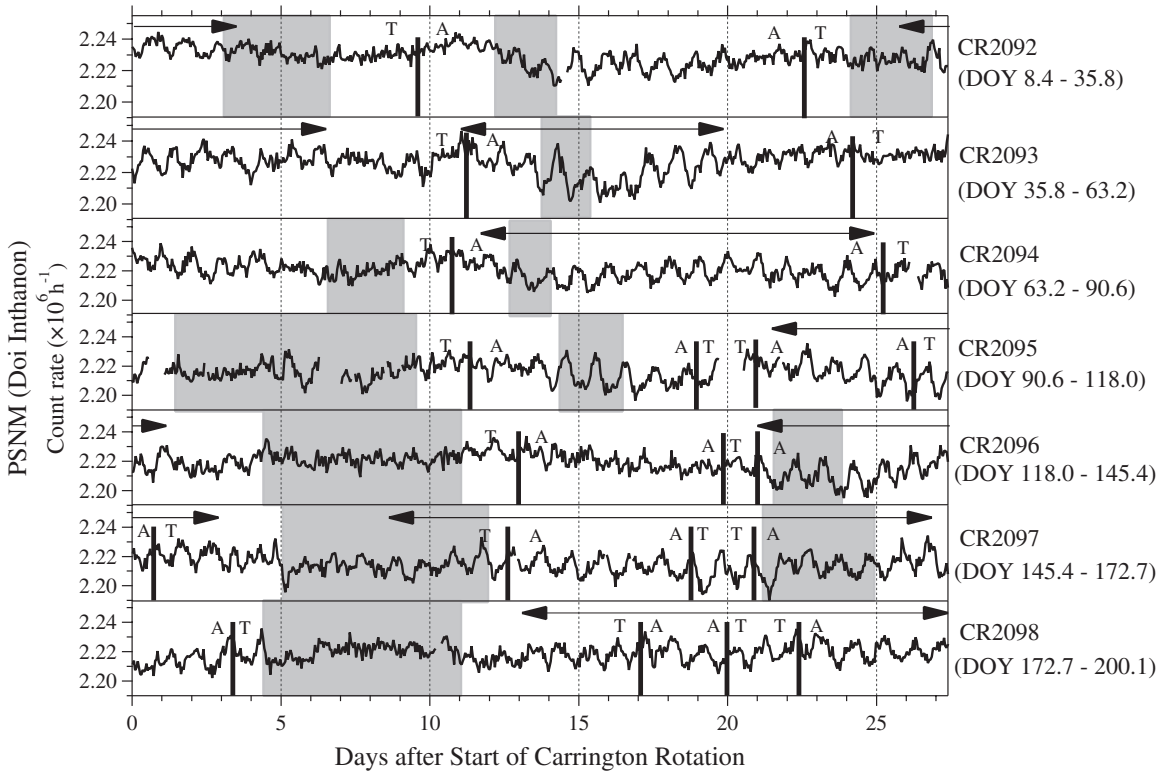

Figure 2. Same as Figure 1 for CR2092–CR2098 during 2010. There are three patterns of enhanced diurnal variations: (1) Enhancement mostly in the T sector during CR2092–CR2093. (2) Repeated enhancement mostly in the A sector, during CR2093–CR2096. (3) Extended enhancements in both the T and A sectors during CR2097–CR2098.

The other time period of recurrent trains of enhanced and suppressed DA, CR2092–CR2098, exhibited more variability in terms of HSSs and DA. There were three types of enhanced diurnal variations, as follows: (1) trains of enhancement mostly in the T sector during CR2092–CR2093, (2) a repeated train of enhancement mostly in the A sector, during CR2093–CR2096, and (3) extended repeated enhancements in both the T and A sectors during CR2097–CR2098.

In summary, during both of these periods of recurrent trains, Figures 1 and 2 show that there were multiple consecutive

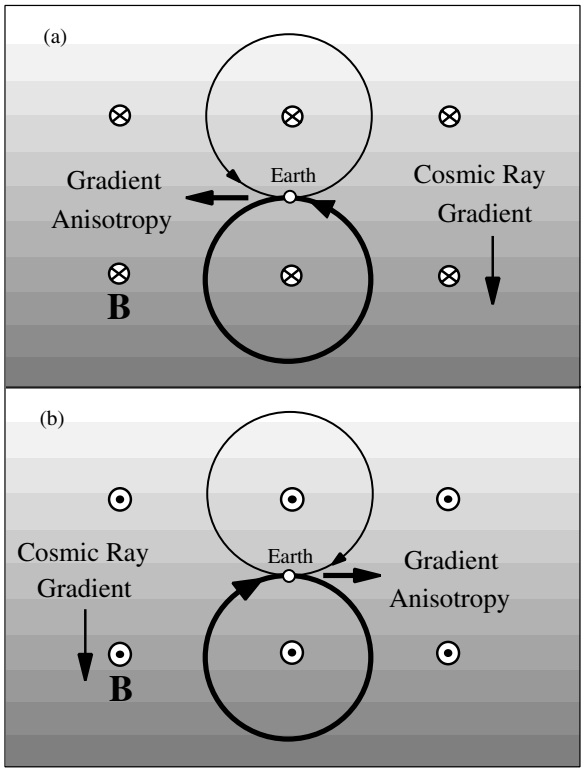

Figure 3. Illustration of the gradient anisotropy. Darker shading indicates a higher cosmic ray density, n, and the gyration of cosmic rays around the interplanetary magnetic field $\mathbf{B}$ leads to a net anisotropy directed along $\mathbf{B} \times \nabla n$. This can explain some changes in the DA that are associated with changes in the sign of $\mathbf{B}$, in which case this figure represents a Sunward view of near-Earth space. When superimposing the normal corotational anisotropy toward the right (along Earth's orbit), a southward gradient in the GCR density leads to (a) suppression or (b) enhancement of the diurnal anisotropy in toward (T) and away (A) magnetic sectors, respectively.

CRs during which the DA was mostly enhanced in the A sectors and suppressed in the T sectors (CR2068–CR2071 and CR2092–CR2095).

3.3. Gradient Anisotropy

As found in the previous section, the DA during the recurrent trains tends to be enhanced or suppressed depending on the sign of the magnetic field $\mathbf{B}$, and was most commonly enhanced during A sectors and suppressed during T sectors. While effects of convection and diffusion do not depend on the sign of $\mathbf{B}$, there is a sign dependence for the gradient anisotropy along $\mathbf{B} \times \nabla n$, which could therefore describe this behavior.

The well-known gradient anisotropy of GCRs along $\mathbf{B} \times \nabla n$ is illustrated by Figure 3. For example, when the cosmic ray density is higher in the southern hemisphere, this provides a southward gradient in the GCR density. The gyration of cosmic rays around the IMF causes an observer to see a net anisotropy along the $\mathbf{B} \times \nabla n$ direction, which is in turn related to the sign of $\mathbf{B}$. As a result, the anisotropy then enhances or suppresses the usual corotational DA in A and T sectors, respectively.

According to Jokipii et al. (1977), the streaming flux is given by $F_i = -\kappa_{ij} \partial n / \partial x_j$, where κ_{ij} is the diffusion-drift tensor and n is the cosmic ray density. This includes a term for the streaming flux due to the gradient (drift) anisotropy, $\mathbf{F}_A = \kappa_A \mathbf{e}_B \times \nabla n$, where $\mathbf{e}_B = \mathbf{B}/B$. Here κ_A describes the antisymmetric part of the diffusion coefficient, including effects of gradient and curvature drifts. For a positive charge and a scattering mean free path much greater than the gyroradius r_g, both of which are true for GCR ions, we have $\kappa_A = v r_g/3$ (Jokipii et al. 1977), where $r_g = \gamma m v / qB = P/cB$, v is the cosmic ray velocity, γ is the Lorentz factor, m is the rest mass, P is the rigidity, and c is the speed of light. The flux $\mathbf{F}_A$ reverses when the particle charge changes sign. An anisotropy is related to the streaming flux as $\mathbf{A} = 3\mathbf{F}/(vn)$ so the anisotropy is $\mathbf{A} = (r_g/n)\mathbf{e}_B \times \nabla n$. If $\mathbf{B}$ is in the ecliptic plane along the x and y directions of GSE coordinates the gradient anisotropy may be expressed as

$$\mathbf{A} = \frac{P}{cB^2 n}\mathbf{B} \times \nabla n = \frac{P}{cB^2 n}\left[\left(B_x \frac{\partial n}{\partial y} - B_y \frac{\partial n}{\partial x}\right)\hat{\mathbf{z}} + (B_y \hat{\mathbf{x}} - B_x \hat{\mathbf{y}})\frac{\partial n}{\partial z}\right]. \quad (3)$$

This expression contains two components of anisotropy. The first term of the right-hand side is the north–south anisotropy (in the $\hat{\mathbf{z}}$ direction) arising from a gradient in the ecliptic plane. This component would make little contribution to the DA. However, the second term is in the ecliptic plane and arises from a latitudinal gradient in GCRs:

$$A_e = r_g \frac{B_e}{B}|G_z|, \quad (4)$$

where the subscript e refers to the magnitude in the ecliptic (x, y) plane, and $G_z = (\partial n/\partial z)/n$ is the fractional latitudinal gradient. A density gradient should cause anisotropy even in a homogeneous magnetic field (Spitzer 1952).

In particular, a southward GCR gradient can explain why the DA was most commonly enhanced in the A sector and suppressed in the T sector. When the magnetic field was in the A sector (usually with $B_x < 0$) in combination with the southward GCR gradient, Equation (3) implies a $\mathbf{B} \times \nabla n$ anisotropy component along $-\hat{\mathbf{y}}$, thus enhancing the usual corotational anisotropy. Similarly, a magnetic field in the T sector (usually with $B_x > 0$) results in a suppression of the corotational anisotropy.

It is interesting to note the large size of the gyroradius for GCRs observed at Doi Inthanon. The angular diameter θ of the gyro-orbit is related to the rigidity by the expression (Subramanian & Sarabhai 1967)

$$\theta \approx \tan^{-1} \frac{2P \sin\alpha}{45B}, \quad (5)$$

where the rigidity P is in GV, the interplanetary field B is in nT, and the look direction α is the direction of motion with respect to the magnetic field (the pitch angle of cosmic rays). The median rigidity P of GCRs observed at Doi Inthanon is about 35 GV (K. Munakata 2010, private communication). On DOY 184 of 2008, a 2 nT field was observed by the *ACE* spacecraft, so for $\alpha = 90°$, at Doi Inthanon a median-rigidity ion had an angular gyro-diameter of $\approx 40°$. Thus the GCR gradient anisotropy at Doi Inthanon can provide information about the gradient over a great distance from the ecliptic plane.

3.4. Case Studies

To study trains of enhanced (or suppressed) DA in more detail, we selected one time period, including the time of maximum DA, from each of the two periods of recurrent trains of enhanced DA, as well as one time period with a non-recurrent train. DAs and phases were also studied in comparison with synoptic maps and interplanetary plasma parameters in order to clarify the mechanism of DA enhancement and suppression.

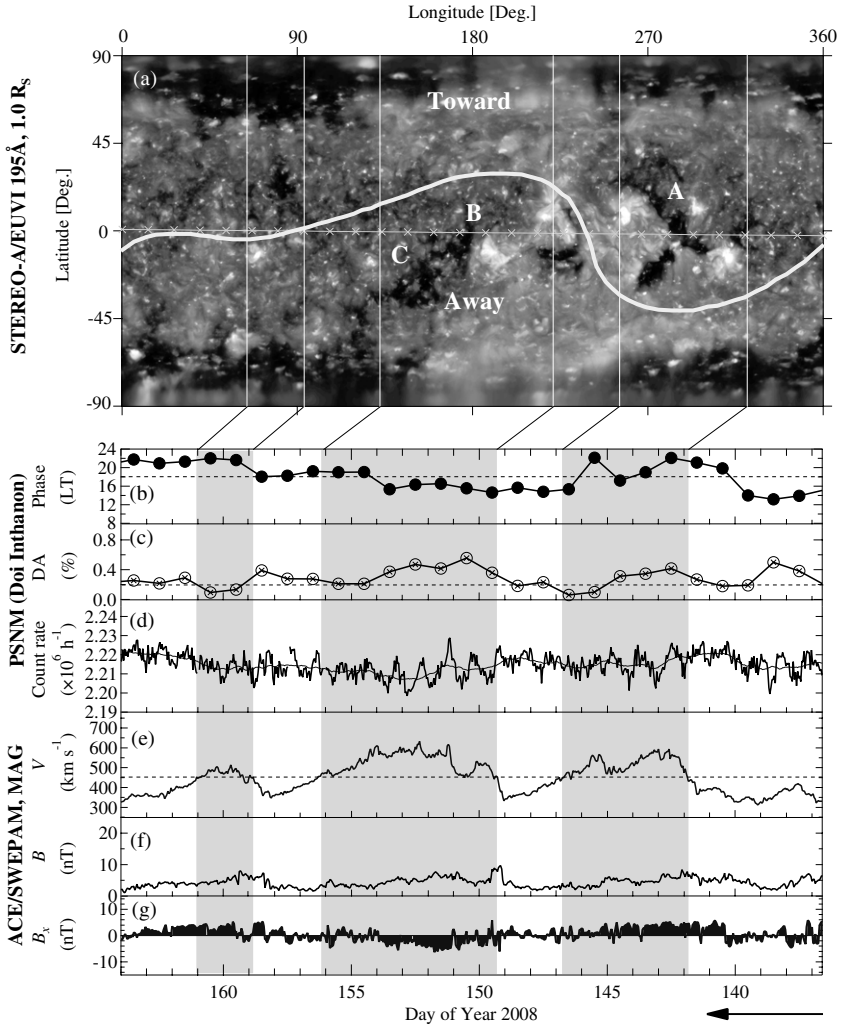

Figure 4. Reversed time plots for Carrington rotation (CR) 2070, from 2008 May 15 to June 11. Data from *STEREO-A*/EUVI: (a) Synoptic map of the solar corona in the Fe XII 195 Å bandpass. The position of the HCS from a WSO synoptic chart is shown by a thick light gray line and the projected orbit of the Earth is indicated by gray crosses. Slanted lines show the correspondence with the reversed time axis of the lower plots. Data from *PSNM*: (b) Phase (time of maximum) of diurnal variation, in local time. The dashed line indicates the corotational anisotropy (1800 LT). (c) Diurnal anisotropy (DA). The dashed line is the observed average DA. (d) Hourly neutron count rate (thick line) and its running 1 day average (thin line). Data from *ACE*: (e) Solar wind speed. (f) Magnitude of magnetic field. (g) Sunward magnetic field component. Shaded areas represent HSSs with speed $\geqslant$450 km s^{-1}. Note the enhanced DA lasting for 5 days starting near the onset of the HSS on day of year (DOY) 149, which we attribute to the slanted geometry of the HSS due to the combined effects of CH B and C. The enhanced DA in the HSS is consistent with the $\mathbf{B} \times \nabla n$ anisotropy for a southward cosmic ray gradient associated with the slanted geometry.

3.4.1. Carrington Rotation 2070 and 2071

We first examine CR2070 and CR2071 (2008 May 15 to July 9), which had recurrent trains of enhanced and suppressed DA, and included the strongest DA found in this study (0.79%). Figures 4 and 5 show reversed-time plots of GCR data from the *PSNM*, together with synoptic maps of the solar corona constructed from Fe XII λ195 images from *STEREO-A*/EUVI, and solar wind plasma parameters from the *ACE* spacecraft. The locations of Earth's orbit (crosses) and latitudinal excursions of the HCS were plotted on the synoptic maps to indicate the source polarity of the IMF. Slanted lines between panels (a) and (b) of each figure show the correspondence between the solar longitude in the synoptic map and the reversed time axis of the lower plots. There is a direct correspondence between magnetic polarity at the Sun (as determined from the location of Earth's orbit relative to the HCS) and predominant polarities of the HSSs (as determined from the magnetic field components B_x, B_y near Earth). The isolated CH ("A") of negative (toward) polarity was located near the solar equator above the HCS, whereas the positive (away) polarity CHs ("B" and "C") were located below the HCS, at the solar equator and southern hemisphere, respectively. During the times of recurrent solar wind streams, there was downward modulation of GCR intensity, heralded by compressions in the magnetic field (B) near Earth at their leading edges.

For one particularly strong sequence of DA enhancement at Doi Inthanon, we can provide a quantitative explanation for a strong southward GCR gradient. The longest-lasting train of enhanced DA was observed for 21 days from DOY 176 (2008 June 24) to DOY 196 (2008 July 14). This time period included the passage of a CIR and HSS with a lower GCR flux during the HSS. The HSS was associated with two positive polarity CHs (see Figure 5; "B" is at the equator and "C" is a mid-latitude extension of the south polar CH). Based on the solar wind speed data, the HSSs are evidently merged to be a compound stream. Indeed, during the preceding CR, CR2070, "B" and "C" formed a merged CH (Figure 4). The compound HSS should therefore be slanted with respect to the solar equator, which should lead to a GCR density gradient perpendicular to its

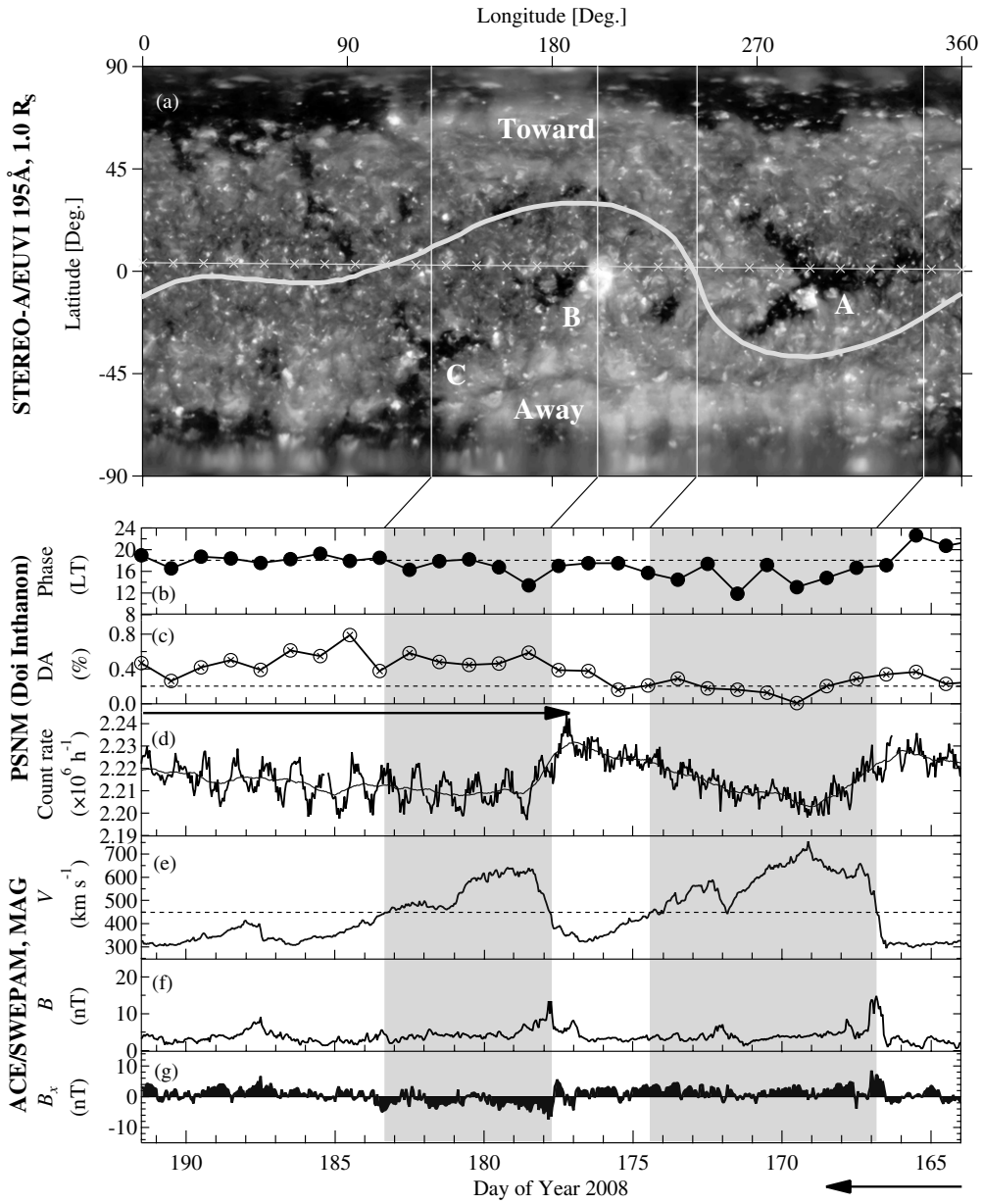

Figure 5. Same as Figure 4 for CR2071, from 2008 June 12 to July 9. Note the train of enhanced DA, indicated by an arrow, starting near onset of a HSS on day of year (DOY) 177, which we attribute to the slanted geometry of the high speed solar wind stream (HSS) due to the combined effects of CHs B and C. The enhanced DA in (c) after the sharp decrease in cosmic ray intensity in (d) is consistent with the $\mathbf{B} \times \nabla n$ anisotropy for a southward gradient associated with the slanted geometry. While the local magnetic field reversed on day 183, the synoptic map (a) indicates that the boundary between toward and away sectors remained near Earth, in comparison with the large gyroradius of cosmic rays observed at Doi Inthanon, so a southward cosmic ray gradient can still contribute to enhanced DA.

boundary. Consequently, the compound HSS from the positive polarity CHs in CR2071 should have a component of latitudinal gradient of cosmic rays toward the south. This should cause an additional anisotropy in the ecliptic plane via the $\mathbf{B} \times \nabla n$ gradient drift flux, as explained in Section 3.3.

To estimate the latitudinal gradient of GCR density, we examined the slope of the decline in the running 24 hr average of the *PSNM* count rate during DOY 177–178 to infer a cosmic ray density gradient of -0.74% day^{-1}. Assuming that the structure moves past the Earth with the synodic period of 26.75 days (Bai 1987), this corresponds to a longitudinal gradient of 3.2% AU^{-1}. Assuming for simplicity that the HSS leading edge is slanted by roughly 30° counter-clockwise from the equatorial plane, like the CH complex (see Figure 4(a)), we infer a latitudinal gradient of -5.5% AU^{-1}. According to Equation (4), if the magnetic field is nearly in the ecliptic plane then $B_e \approx B$ and $A_e \approx r_g|G_z|$ (Datter & Venkatesan 1959). For median rigidity protons detected by *PSNM*, at 35 GV, the Larmor radius was about 0.1 AU for the average magnetic field, 7 nT, near the leading edge of the HSS during DOY 177–178, and from $G_z = -5.5\%$ AU^{-1} the gradient anisotropy should be about 0.55%, which is in good agreement with the observed enhancement in the DA.

In the A sector, the average DA was $0.50\% \pm 0.10\%$ and the phase was 17.5 ± 1.4 hr LT. In the T sector, they were $0.19\% \pm 0.09\%$ and 15.6 ± 2.0 hr LT in the first half of the CR. From these values we see that the DAs are different, but the average phases are consistent with the corotational direction of 18 hr LT (although in the T sector there was a larger spread). This is in contrast with the results reported by Mavromichalaki

(1989) and Mishra & Mishra (2005) for GCR at lower energy.

In Section 3.2, we discussed that the recurrent trains during CR2068–CR2073 included two types of trains, starting in the A sector (CR2068, CR2069, CR2071, and CR2072) or the T sector (CR2072 and CR2073), as seen from Figure 1. The earlier portion, CR2068–CR2071, exhibits mainly enhanced DA during A sectors and suppressed DA during T sectors, which is well explained by a gradient anisotropy associated with a general southward gradient in the GCR density. In contrast, CR2072 and CR2073 contain T-sector trains of enhanced DA that are not explained by the effect of a southward GCR gradient. These two T-sector trains, associated with CH "A," could have had a northward GCR gradient in CR2072 and CR2073, or could have had an enhanced DA due to other processes such as a combination of convection and diffusion.

CR2071 presents an interesting case where the two types of trains merge into a 21 day train over DOY 176–196. This is the only train in our survey that lasted more than 14 days. After the very strong DA in the A sector during DOY 176–185, which we attribute to a slanted compound HSS due to CH "B" and "C" and the resulting strong southward GCR gradient south of the HCS that leads to a strong gradient anisotropy, it is notable that the DA was still high in the T sector during the recovery of the GCR flux on DOY 186–191. That is still consistent with a southward GCR gradient because the HCS was close to the solar equator. Recalling that the gyro-orbits of GCRs are very large in this rigidity range (see Section 3.3), the gradient anisotropy can result from gradients over a large distance. Indeed, when the HCS is close to Earth in comparison with the particle gyroradius, with an A sector to the south and a T sector to the north, both a southward gradient south of the HCS (due to the CH "B" and "C") and a northward gradient north of the HCS (due to CH "A") can contribute to enhanced DA. We suggest that the effects of the two sets of CHs overlapped in solar longitude while the HCS was close to Earth, leading to this continuous train of enhanced DA.

3.4.2. Carrington Rotation 2093

Now we turn to the other period of recurrent trains of enhanced DA, in 2010. As shown in Figure 6, CR2093 (2010 February 4 to March 4) exhibited two trains, a non-recurrent train that started during an HSS in the T sector during DOY 34–42, and a train during DOY 48–56 that recurred in subsequent CRs in association with the A sector of the IMF near Earth. The strongest DA was 0.75%, which was the greatest value observed in 2010. Throughout CR2092–CR2095, the DA was mostly enhanced in the A sectors and suppressed in the T sectors. A gradient anisotropy could explain this association with the sign of **B**, which would again require a southward GCR gradient.

We also found a correspondence between polarities of the CHs and the HSSs. A complex CH structure of negative polarity was located far above the solar equator and the HCS, whereas a large stripe of positive polarity CHs was located in the southern hemisphere. Around DOY 48–53, the GCR intensity was clearly reduced during the passage of a HSS that emerged from an isolated positive equatorial CH at longitude about 160°. It is notable that the greatest reduction in GCR intensity and the highest levels of the DA were close to the region of the HSS. Note also that the DA was enhanced during the passage of the moderate HSS in the A sector, but tended to diminish close to the boundaries with the T sector.

In the A sector, the average DA was $0.47\% \pm 0.20\%$ and the phase was 15.6 ± 1.1 hr LT. In the T sector, the average DA was $0.29\% \pm 0.15\%$, mainly in association with the non-recurrent T-sector DA enhancement, and the phase was 16.6 ± 1.8 hr LT. Interestingly, the phase of the diurnal variation was generally low during this CR.

3.4.3. Carrington Rotation 2064

Now we consider an example of a non-recurrent train of enhanced DA in CR2064 (2007 December 3 to December 30) for which we again found a correspondence between polarities of the CHs and the HSSs (Figure 7). An isolated CH of negative polarity ("A") was located at the solar equator and near the HCS, whereas a largely slanted positive polarity CH structure ("B") was located in the southern hemisphere. Observationally, the larger CH "B" provided a broader HSS region in interplanetary space than the CH "A."

Around DOY 345–358, the GCR intensity was clearly reduced during the passages of the two HSSs from CH "A" and "B." As usual, the higher solar wind speed can inhibit the GCR flux. The two CHs were close to each other, so the GCR intensity could not effectively recover around DOY 349 to the previously level as on DOY 343–344. The GCR intensity did clearly recover around DOY 362 behind the passage of the HSS from CH "B."

Of the two HSSs, only the latter was associated with a train of enhanced DA. This started during the passage of the large HSS with a complex velocity profile associated with CH "B" in the A sector and lasted for 9 days, DOY 351–359. As described before for CR2071, the slanted structure of the CH ("B") can provide a latitudinal gradient of GCRs toward the south that should cause an enhanced DA by the $\mathbf{B} \times \nabla n$ gradient anisotropy in the A sector. The lower value of the average enhanced DA during this CR should be related to the much lower GCR gradient seen in the *PSNM* count rate. In the A sector of CR2064, the average DA was $0.34\% \pm 0.13\%$ and the average phase was 16.7 ± 2.1 hr LT, whereas in the T sector, the DA was $0.24\% \pm 0.09\%$, which is consistent with the average value during our 3 yr survey, and the phase was 17.8 ± 2.7 hr LT. We can see that the average phases were close to the corotational direction in both magnetic sectors.

It is notable that DA values in the trains of enhanced DA were different during the passage of the CIR and HSS in Figures 5 and 7, especially in the trailing part of the HSSs. In CR2064 around DOY 356–358 and in CR2071 around DOY 184–186, the DAs were higher than they were near the CIR. The greatest enhancement occurred at times when the corresponding CHs were located at heliolatitudes of about 40°–50°. As the CIR structure extended to high latitudes because of the slanted morphology of CHs, the latitudinal gradient of GCRs also extended to those high latitudes. In the context of $\mathbf{B} \times \nabla n$ anisotropy, we are able to explain some features of enhanced and suppressed DA in association with a latitudinal gradient of GCRs over a domain that has the dimensions of the gyroradius of the cosmic ray particles.

4. SUMMARY

In this work we have characterized and analyzed the effects of CHs and HSSs on enhanced diurnal variation of GCRs as observed by a neutron monitor at Doi Inthanon, Thailand with cutoff rigidity of 16.8 GV during a 3 yr period in the recent solar minimum. We observed numerous consecutive trains of

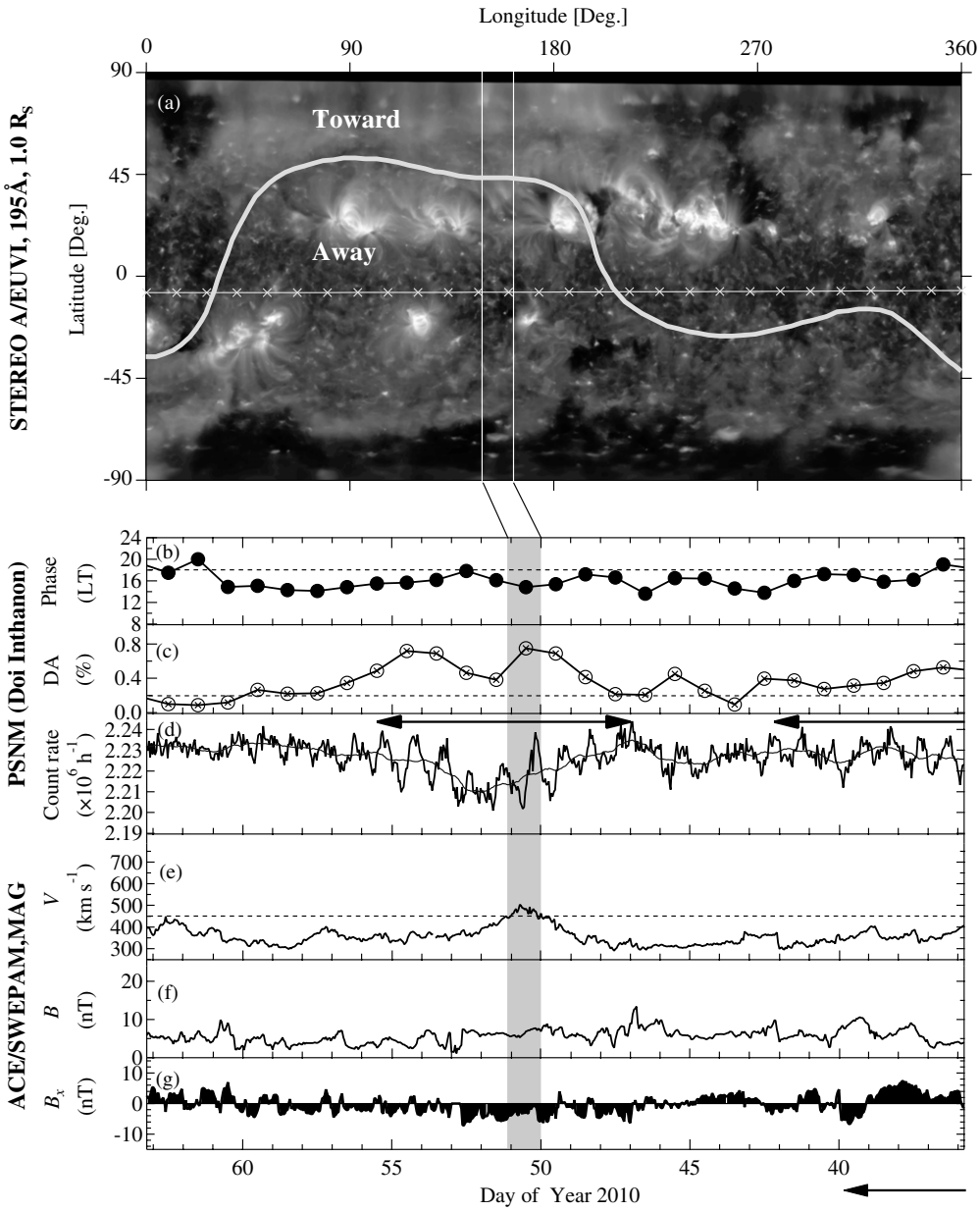

Figure 6. Same as Figure 4 for CR2093, from 2010 February 4 to March 4. This is an example of a recurrent train of enhanced DA in 2010, in association with the away sector of the interplanetary magnetic field near Earth. A gradient anisotropy could explain this association, although the reason for a southward GCR gradient is not clear.

enhanced DA that lasted more than seven days, and found that these trains often recurred after a solar rotation period. The suppression and enhancement of DA were mainly in the T and A sectors of the IMF, respectively. This "odd" dependence on the sign of the IMF is in contrast with the "even" dependence in drift models of solar modulation that stress a symmetric role of the HCS (Kóta & Jokipii 2001).

The long-lasting trains of enhanced DA were observed after the passages of some but not all CIRs. After a CIR and within an HSS, there is usually a lower density of GCRs. Such decreases lead to the well-known 27 day variations in which CHs rotate with the Sun and the associated HSSs return with the rotation period of ∼27 days, leading to recurrent decreases in the GCR flux. The GCR decreases have been attributed to either shielding by the GCR or changes in the cosmic ray diffusion tensor.

During most time periods of recurrent trains of enhanced DA (i.e., CR2068–CR2071 and CR2092–CR2095), the DA was enhanced during the A magnetic sector and suppressed during the T magnetic sector. We propose that the most natural explanation for this is a gradient anisotropy, associated with a southward GCR gradient, that either enhanced or suppressed from the usual corotational anisotropy when the magnetic field was outward or inward, respectively. Previous work has remarked on the importance of the gradient anisotropy associated with a density gradient of GCRs in the inner heliosphere for the DA averaged over long time periods (Hashim & Bercovitch 1972; Owens et al. 1980; Bieber & Chen 1991; Chen & Bieber 1993) or short time periods (Bieber & Evenson 1998; Kuwabara et al. 2004, 2009). In our data, the very strongest enhancement was associated with a slanted HSS, which can account for a particularly strong GCR gradient and the particularly strong DA.

More generally, trains of enhanced DA commonly occurred near the time of a sudden GCR decrease (see Figures 1 and 2). In all such cases, there was a strong GCR gradient, and as the

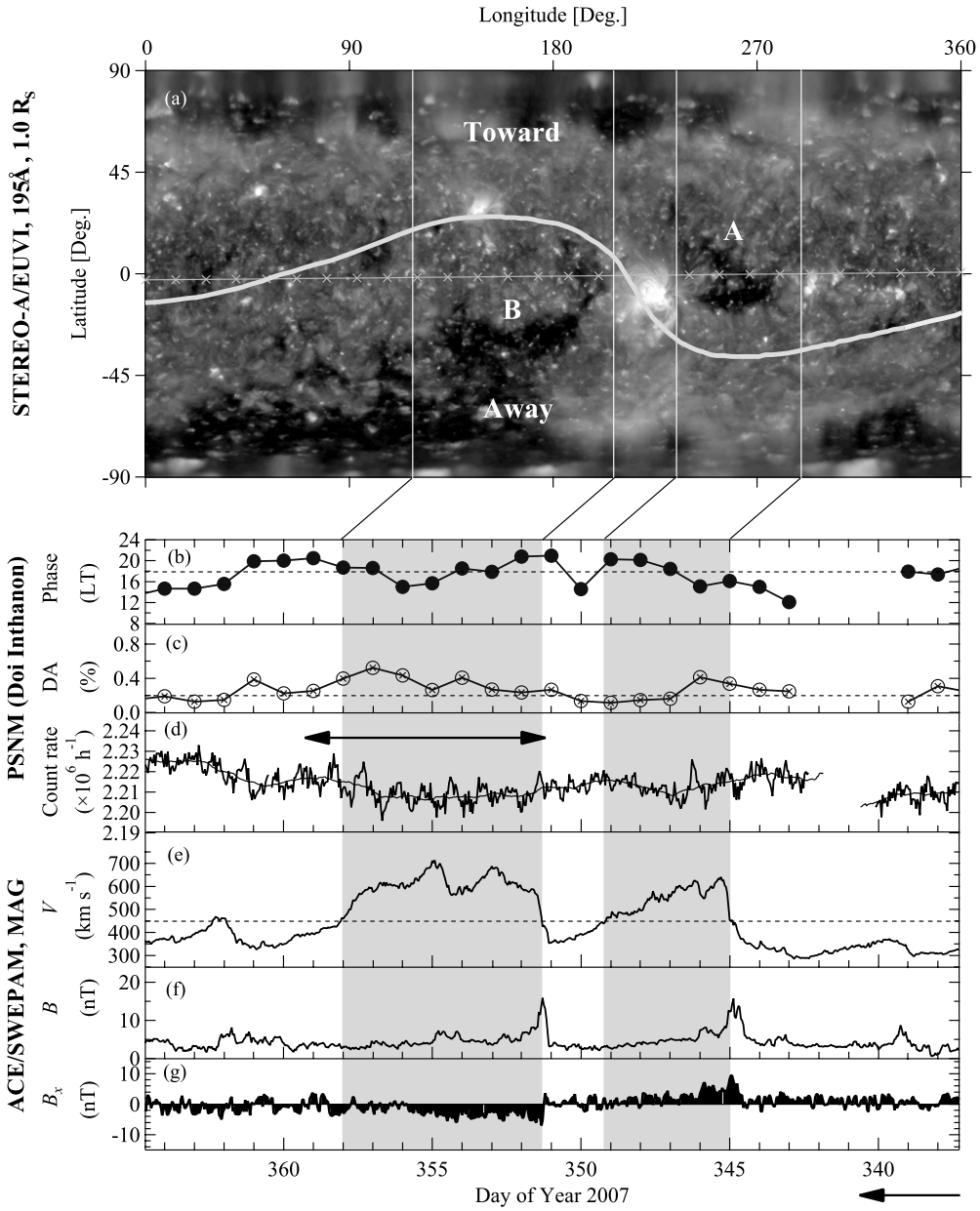

Figure 7. Same as Figure 4 for CR2064, from 2007 December 3 to December 30. An example of a non-recurrent train of enhanced DA in 2007, which is also associated with the away sector of the magnetic field and could also be explained by a gradient anisotropy.

boundary of the GCR-depleted region (roughly corresponding to an HSS) is more likely to be slanted than to be perfectly north–south aligned, it is likely that a north–south gradient exists and plays a role in the DA enhancement through the gradient anisotropy.

For detailed case studies, we have selected one time period, including the time of maximum DA, from each of the two recurrent trains of enhanced DA (CR2070–CR2071 and CR2093), and one time period with a non-recurrent train (CR2064). We find that in CR2071 (and subsequent events) and CR2064, the HSS from an equatorial CH merged with that from a trailing mid-latitude extension of the south polar CH to produce a slanted HSS structure in space, within which the cosmic ray density was depressed. This can lead to a particularly strong local latitudinal gradient as the GCR intensity was reduced in the HSS region. The latitudinal gradient of GCRs can be estimated from the angle of the slanted structure and the rate of decrease in the GCR flux at Doi Inthanon. The inferred gradient anisotropy is consistent with magnitude of the temporary enhancement of the DA.

The slanted geometry of CHs plays a role in enhancing the DA in the A sectors when the latitudinal gradient points to the south. The slanted structure was quite flat in CR2067, but more slanted in the subsequent recurrences in CR2068–CR2072 (see Figure 5). In addition, the slanted geometry of CHs disappeared in CR2073 which immediately followed the last recurrent trains of enhanced DA in the A sector (Figure 1). These observations confirm that the slanted geometry of CHs can enhance the latitudinal gradient and the gradient anisotropy contribution to the DA.

We are grateful to Thai Ministry of Science and Technology for support and funding. This research was partially supported by the Thailand Research Fund. We thank Takao Kuwabara and Kazuoki Munakata for useful discussions. The

STEREO/SECCHI data are produced by a consortium of NRL (US), LMSAL (US), NASA/GSFC (US), RAL (UK), UBHAM (UK), MPS (GM), CLS (Belgium), IOTA (France), and IAS (France). We thank the *ACE* SWEPAM and MAG instrument teams and the ACE Science Center for providing the *ACE* data.

REFERENCES

Agrawal, S. P., Lanzerotti, L. J., & Venkatesan, D. 1978, JGR, 5, 589
Agrawal, S. P., Lanzerotti, L. J., Venkatesan, D., & Hansen, R. T. 1980, JGR, 85, 6845
Bai, T. 1987, ApJ, 314, 795
Bieber, J. W., & Chen, J. 1991, ApJ, 372, 301
Bieber, J. W., & Evenson, P. 1998, GeoRL, 25, 2955
Burlaga, L. F. 1974, JGR, 79, 3717
Chen, J., & Bieber, J. W. 1993, ApJ, 405, 375
Chih, P. P., & Lee, M. A. 1986, JGR, 91, 2903
da Silva, M. R., Dal Lago, A., Echer, E., et al. 2007, AdSpR, 40, 348
Datter, A., & Venkatesan, D. 1959, Tell, 11, 239
Duldig, M. L., & Humble, J. E. 1990, PASA, 8, 268
Fonger, W. H. 1953, PhRv, 91, 351
Forman, M. A., & Gleeson, L. J. 1975, Ap&SS, 32, 77
Gil, A., Modzelewska, R., & Alania, M. V. 2012, AdSpR, 50, 712
Hashim, A., & Bercovitch, M. 1972, P&SS, 20, 791
Heber, B., Sanderson, T. R., & Zhang, M. 1999, AdSpR, 23, 567
Hess, V. F., & Graziadei, H. Th. 1936, TeMAE, 41, 9
Howard, R. A., Moses, J. D., Vourlidas, A., et al. 2008, SSRv, 136, 67
Hundhausen, A. J., Sime, D. G., & Hansen, R. T. 1980, Sci, 207, 761
Iucci, N., Parisi, M., Storini, M., & Villoresi, G. 1983, NCimC, 6C, 145
Jokipii, J. R., Levy, E. H., & Hubbard, W. B. 1977, ApJ, 213, 861
Kaiser, M. L., Kucera, T. A., Davila, J. M., et al. 2008, SSRv, 136, 5
Kóta, J., & Jokipii, J. R. 1991, GeoRL, 18, 1797
Kóta, J., & Jokipii, J. R. 2001, AdSpR, 27, 607
Kuwabara, T., Bieber, J. W., Evenson, P., et al. 2009, JGR, 114, 5109
Kuwabara, T., Munakata, K., Yasue, S., et al. 2004, GeoRL, 31, 19803
Lin, Z., Bieber, J. W., & Evenson, P. 1995, JGR, 100, 23543
Mavromichalaki, H. 1989, EM&P, 47, 61
Mishra, R. K., & Mishra, R. A. 2005, P&SS, 53, 739
Mori, S., Yasue, S., Ichinose, M., & Munakata, Y. 1975, in Proc. 14th ICRC (München), 4, 1463
Munakata, Y., Darwish, A., Fujii, Z., Kato, C., & Mori, S. 2003, in Proc. 28th ICRC (Tsukuba), 7, 3925
Nagashima, K., Sakakibara, S., & Murakami, K. 1989, NCimC, 12C, 173
Owens, A. J., Duggal, S. P., Pomerantz, M. A., & Tolba, M. F. 1980, ApJ, 236, 1012
Pomerantz, M. A., & Duggal, S. P. 1971, SSRv, 12, 75
Rao, U. R. 1972, SSRv, 12, 719
Richardson, I. G. 2004, SSRv, 111, 267
Schatten, K. H., Wilcox, J. M., & Ness, N. F. 1969, SoPh, 6, 442
Simpson, J. A. 1998, SSRv, 83, 169
Singh, A., Tiwari, A. K., & Agrawal, S. P. 2010, JApA, 31, 89
Spitzer, L., Jr. 1952, ApJ, 116, 299
Subramanian, G., & Sarabhai, V. 1967, ApJ, 149, 417
Zirker, J. B. 1977, RvGSP, 15, 257